

HYDROGEN MOLECULES IN THE DARK AGES HALOS: THERMAL EMISSION VS. RESONANT SCATTERING

B. NOVOSYADLYJ^{1,2}, V. SHULGA^{1,3}, YU. KULINICH², W. HAN¹

¹College of Physics and International Center of Future Science of Jilin University, Qianjin Street 2699, Changchun, 130012, P.R.China,

²Astronomical Observatory of Ivan Franko National University of Lviv, Kyryla i Methodia str., 8, Lviv, 79005, Ukraine,

³Institute of Radio Astronomy of NASU, 4 Mystetstv str., 61002 Kharkiv, Ukraine

Submitted to ApJ

ABSTRACT

The emission from dark ages halos in the lines of transitions between lowest rotational levels of hydrogen and hydrogen deuteride molecules is analyzed. It is assumed molecules to be excited by CMB and collisions with hydrogen atoms. The physical parameters of halos and number density of molecules are precalculated in assumption that halos are homogeneous top-hat spheres formed from the cosmological density perturbations in the four-component Universe with post-Planck cosmological parameters. The differential brightness temperatures and differential spectral fluxes in the rotational lines of H₂-HD molecules are computed for two phenomena: thermal luminescence and resonant scattering of CMB radiation. The results show that expected maximal values of differential brightness temperature of warm halos ($T_K \sim 200$ -800 K) are at the level of nanokelvins, are comparable for both phenomena, and are below sensitivity of modern sub-millimeter radio telescopes. For hot halos ($T_K \sim 2000$ -5000 K) the thermal emission of H₂-ortho molecules dominates and the differential brightness temperatures are predicted to be of a few microkelvins at the frequencies 300-600 GHz, that could be detectable with telescopes of a new generation.

Subject headings: cosmology: theory — galaxies: formation — galaxies: high-redshift — stars: formation hydrodynamics — intergalactic medium

1. INTRODUCTION

Formation of the first luminous objects of the Universe is important topic of current cosmology. It is the generally accepted paradigm that they are formed from the initial small matter density and velocity perturbations generated at the early stages of the evolution of the Universe. The most interesting stages of their early evolution are hidden in the Dark Ages, period of time between the last scattering of the cosmic microwave background (CMB) at $z \approx 1000$ and reionization of the intergalactic medium by early luminous objects at $z \approx 10$ (Planck Collaboration 2018a). The theories of generation and evolution of cosmological perturbations successfully describe the observed anisotropy of CMB and the large-scale structure of the Universe that make it possible to evaluate the basic parameters of the cosmological model of the Universe and the ratio of the densities of its main components such as baryonic matter, dark matter and dark energy, with sufficient accuracy. The lowest scales in these theories, which are probed by observations, are dozens of Megaparsecs in current astronomical units that are essentially larger than expected ones for the first luminous objects, stars, globular clusters or dwarf galaxies. The numerical simulations of the large-scale structure formation at these scales are very complicated and ambiguous because the non-linear dynamical effects in the multi-component medium, gas-dynamics, molecular chemistry and cooling/heating processes become important or even key. The considerable ambiguity of the predictions of the theoretical simulations at these scales is due also to the uncertainty of the physical nature of dark matter and dark energy. This supports the importance of analyzing the possibilities of detection of signals from Dark Ages both in the line of 21 cm of atomic hydrogen and in the lines of the first molecules.

The theoretical investigations of the possible signal

from the Dark Ages in the hyperfine structure line 21 cm of atomic hydrogen are intensive and already have long history (see, for example, reviews Barkana et al. (2001); Fan et al. (2016); Furlanetto et al. (2006); Pritchard & Loeb (2012)). It was predicted that an expected signal at ~ 100 MHz can be at the level of hundreds - dozens of millikelvins of brightness temperature. It seems that the long-term efforts of several scientific groups to detect such signal from the Dark Ages gave finally the first results: the team of the Experiment to Detect the Global EoR Signature¹ (EDGES) has announced the registration of absorption line 21 cm of atomic hydrogen with the brightness temperature about 0.5 K at $z = 15$ -20 (Bowman et al. 2018). Unfortunately the signal in the molecular lines is expected rather weaker but it can be more informative since it can say about molecular chemistry and physical conditions of excitation of lines. The upper limits for such signal at the level of few millikelvins have been obtained in a few observations by IRAM 30 m telescope (de Bernardis et al. 1993), RATAN-600 (Gosachinskij et al. 2002) and the Odin satellite (Persson et al. 2010).

The molecular line signals from the Dark Ages can be observed in the emission or in absorption on the background of the CMB radiation, that is defined by competition of excitation/de-excitation of levels by the CMB radiation and the local sources of radiation or collisions with particles. So, the local physics conditions in the baryonic matter of Dark Ages may cause the secondary anisotropy of CMB. This mechanism is known as thermal emission/absorption and it is like to photo- or thermoluminescence in the solids (Chen & McKeever 1997). The emission in the rotational lines of H₂ and HD molecules from the forming Population III objects and protogalax-

¹ <https://www.haystack.mit.edu/ast/arrays/Edges/>

ies in Dark Ages have been studied by Kamaya & Silk (2002, 2003); Omukai & Kitayama (2003); Mizusawa et al. (2005) and other authors. The marginal possibility of their detection by current and future facilities and their importance have been discussed by them too. The gas clouds or halos which have large peculiar velocity along the line of sight are another source of secondary anisotropy: the resonant scattering of CMB quanta by molecules in the moving halos may cause increasing or decreasing of the brightness temperature of the radiation passing through the halo depending on the direction of peculiar velocity relative to the observer. It was predicted by Dubrovich (1977) and possibility of its observation were studied in Maoli et al. (1994, 1996); Dubrovich et al. (2008); Núñez-López et al. (2006); Persson et al. (2010) and other papers.

The gas in the halos, which have been virialized at $10 \leq z \leq 50$, is over-densed and re-heated (Novosyadlyj et al. 2018): the range of matter density is $\sim 10^{-24} - 10^{-22}$ g/cm³, the range of gas temperature heated adiabatically is $\sim 50 - 800$ K, heated by shocks in the processes of violent relaxation to virial temperature is $\sim 10^4 - 10^5$ K. Hence, the dark ages halos can be a detectable source of thermal emission in the molecular lines of the most abundant molecules H₂ and HD. In the paper we estimate the brightness temperature of molecular lowest rotational energy levels emission from dark ages halos under the condition of radiative and collisional excitation.

The outline of this paper is as follows. In section 2 we briefly describe the models of halos, their physical characteristic and chemical composition. In section 3 we describe the computations of the rates of collisional excitations of the lowest five rotational levels of hydrogen molecules by atomic hydrogen and estimate the critical number density of perturbers. The methods of computations of populations and excitation temperatures of these levels are presented in section 4. In section 5 we present the results of computations of opacity, differential brightness temperatures and differential spectral fluxes caused by thermal collisions of hydrogen molecules with hydrogen atoms. In section 6 we compute for the same halos and lines the differential brightness temperatures and fluxes caused by the resonant scattering of the CMB radiation. Conclusions are in section 7.

The table with data for all halos analyzed in the paper, tables with coefficients of interpolations, tables with the main results and animate figures with evolution of opacities and differential brightness temperatures for halos of different mass are presented in the Appendix of the on-line version.

2. MODELS OF DARK AGES HALOS

We set the physical conditions and chemistry of the halos by modeling the evolution of individual spherical perturbations in the four-component Universe (cold dark matter, baryon matter, dark energy, and thermal relict radiation) starting from the linear stage at the early epoch, through the quasi-linear stage, turnaround point and collapse up to virialized state (Novosyadlyj et al. 2016, 2018). All physical values and chemical composition of a halo with mass $M_h = 5.3 \cdot 10^9 M_\odot$, which are necessary for computation of the excitations and brightness temperatures in the molecular rotational lines, are presented in Table 1. The data for halos of other mass,

$6.6 \cdot 10^8$, $8.3 \cdot 10^7$, $1.0 \cdot 10^7$ and $1.3 \cdot 10^6 M_\odot$, are presented in Table 11 in Appendix of the on-line version.

All computations in the paper are performed for consistent values of the main parameters of the cosmological model, namely, the Hubble constant $H_0 = 70$ km/s/Mpc, the mean density of baryonic matter in the units of critical one $\Omega_b = 0.05$, the mean density of dark matter $\Omega_m = 0.25$, the mean density of dark energy $\Omega_{de} = 0.7$, its equation of state parameter $w_{de} = -0.9$, the effective sound speed $c_s = 1$ (in units of speed of light). The models with dark energy with $w = const$ and cold dark matter (CDM) often are noted as Λ CDM. The dark matter can be also warm dark matter (WDM) with mass of particles larger than a few keV.

We suppose that halo is spherical and homogeneous (top-hat) with values of matter density, kinetic temperature and the number density of species obtained from the computations of its formation. The mass of each halo M_h in the solar mass, its radius in comoving coordinates r_h [kpc] and the wave number k [Mpc⁻¹] of initial perturbation from which halo is formed, are connected by relations

$$\frac{M_h}{M_\odot} = 1159 \Delta_v (1 + z_v)^3 \Omega_m h^2 r_h^3 = 4.5 \cdot 10^{12} \Omega_m h^2 k^{-3},$$

where z_v is the redshift of halo virialization, $\Delta_v \equiv \rho_m(z_v)/\bar{\rho}_m(z_v)$, $\Omega_m \equiv \bar{\rho}_m(0)/\rho_{cr}(0)$, $h \equiv H_0/100$ km/s/Mpc. They are presented in Table 1 and 11. The angular sizes of analyzed halos are in the range $\sim 0.06 - 1.25$ arcsec (last columns of tables 1 and 11). In the computations we assume $\Delta_v = 178$.

The values of matter density, kinetic temperature of baryon component and radius of halo, presented in Table 1, do not change after virialization. The number density of neutral hydrogen atoms (n_{HI}) is practically unchanged, while the number densities of molecules, protons (n_p) and electrons (n_e) are monotonically changed since molecular reactions continue. Therefore, we present their values in Table 1 and 11 at z_v and $z = 10$, in the computations we use the model values at any z .

3. RATES OF EXCITATION/DE-EXCITATION OF ROTATIONAL LEVELS OF H₂ AND HD

In this paper we analyze the possible line emission of molecules H₂ and HD caused by spontaneous transitions between the lowest rotational levels with quantum numbers $J = 0, 1, \dots, 5$ in the dark ages halos before reionization at $z \geq 10$. They can be excited by quanta of CMB, collisions of these molecules with atoms and molecules, and slight light background of first stars at the end of Dark Ages. The rotational quantum numbers of allowed transitions $J_u - J_l$, Einstein coefficients A_{ul} , frequencies ν_{ul} and energy of levels² E_u of molecules H₂ and HD are presented in Table 2.

The collisional excitations are crucially important since they make a possibility to separate the luminous of halos from the CMB background, by other words, to detect them. The bases of the theory of collisional excitation of lowest rotational levels of molecules, which are important for observational radioastronomy, have been initiated in the papers Purcell (1952); Takayanagi & Nishimura (1960); Takayanagi (1963); Field et al. (1966);

² <http://www.cv.nrao.edu/php/splat/advanced.php>

TABLE 1

PHYSICAL VALUES AND CHEMICAL COMPOSITION OF HALOS VIRIALIZED AT DIFFERENT z_v : M IS THE TOTAL MASS, C_k IS THE AMPLITUDE OF INITIAL CURVATURE PERTURBATION (SEED OF HALO), z_v IS THE REDSHIFT OF VIRIALIZATION, ρ_m IS THE MATTER DENSITY VIRIALIZED HALO, T_K IS KINETIC TEMPERATURE OF BARYONIC GAS, n_{HI} IS THE NUMBER DENSITY OF NEUTRAL HYDROGEN ATOMS, n_p , n_e ARE THE NUMBER DENSITIES OF PROTONS AND ELECTRONS AT $z = z_v/10$, n_{H_2} AND n_{HD} ARE THE NUMBER DENSITIES OF MOLECULES H_2 AND HD, r_h IS THE RADIUS OF HALO IN COMOVING COORDINATES, θ_h IS THE ANGULAR RADIUS OF GEOMETRICALLY LIMITED HALO.

M_h	k	C_k	z_v	ρ_m	T_K	n_{HI}	$n_p \approx n_e$	n_{H_2}	n_{HD}	r_h	θ_h
[M_\odot]	[Mpc $^{-1}$]			[g/cm 3]	[K]	[cm $^{-3}$]	[10 $^{-6}$ cm $^{-3}$]	[10 $^{-6}$ cm $^{-3}$]	[10 $^{-9}$ cm $^{-3}$]	[kpc]	[arcsec]
$5.3 \cdot 10^9$	5	$3.0 \cdot 10^{-4}$	30.41	$1.52 \cdot 10^{-23}$	402.1	1.14	106.2/3.8	14.39	2.51	1.78	1.03
		$2.5 \cdot 10^{-4}$	25.15	$8.79 \cdot 10^{-24}$	298.9	0.66	66.1/4.0	5.99	2.07	2.14	1.05
		$2.0 \cdot 10^{-4}$	19.90	$4.49 \cdot 10^{-24}$	206.3	0.34	36.7/4.0	2.15	1.51	2.68	1.09
		$1.5 \cdot 10^{-4}$	14.65	$1.89 \cdot 10^{-24}$	124.3	0.14	17.0/4.4	0.63	0.52	3.60	1.15
		$1.0 \cdot 10^{-4}$	9.41	$5.55 \cdot 10^{-25}$	59.8	0.04	5.6/5.0	0.13	0.08	5.38	1.26

TABLE 2

THE VALUES OF SPONTANEOUS TRANSITIONS ALLOWED BY QUANTUM SELECTION RULES, FREQUENCIES AND ENERGY FOR THE LOWEST FIVE ROTATIONAL ENERGY LEVELS OF HYDROGEN MOLECULES H_2 AND HYDROGEN DEUTERIDE MOLECULES HD.

Species	Transitions ^a	A_{ul}	Frequency ν_{ul}	E_u
	$J_u - J_l$	[s $^{-1}$]	[GHz]	[K]
H_2	2-0	2.94×10^{-11}	10621	510
	3-1	4.76×10^{-10}	17594	1015
	4-2	2.75×10^{-9}	24410	1681
	5-3	9.83×10^{-9}	31011	2503
HD	1-0	5.32×10^{-8}	2675	128
	2-1	5.05×10^{-7}	5332	384
	3-2	1.80×10^{-6}	7952	766
	4-3	4.31×10^{-6}	10518	1271
	5-4	8.35×10^{-6}	13015	1895

^aHere and below u means upper level, l means lower level

Rogers & Barrett (1968); Goss & Field (1968). The computations of excitation/de-excitation rate of lowest ro-vibrational levels of molecules H_2 by collisions with hydrogen atoms have been done by Flower (1997, 1998); Wrathmall et al. (2007); Lique et al. (2012); Lique (2015). The data by Flower (1997, 1998); Wrathmall et al. (2007) contain the rate coefficients of collision transitions between ro-vibrational levels with $\Delta J = \pm 2, \pm 4, \dots$ up to 26th level for both spin isomers ortho- and para-hydrogen molecule. They are available at the Ro-Vibrational Collisional Excitation Database of VAMDC consortium³ as well as the analytical fits of their dependences on temperature which are enough accurate for the temperature range 100-6000 K. We use these fits for the de-excitation rate coefficients of para-/ortho- H_2 by atomic hydrogen for $T_K \geq 100$ K, for the lower temperatures we use the extrapolation by second-order polynomial on the base of nearest three datapoints. The coefficients for fits and extrapolations of collisional deexcitation κ_{ul} of lowest rotational levels of molecules para- H_2 ($J = 0, 2, 4$) and ortho- H_2 ($J = 1, 3, 5$) used here are presented in Appendix of the on-line version in Tables 12 and 13 accordingly. The collisional excitation rate coefficients κ_{lu} are computed using the well known relation $\kappa_{lu} = \kappa_{ul}g_u/g_l / \exp(h\nu_{ul}/kT_K)$. The dependences of coefficients of collisional rate excitation/de-excitations

of three lowest levels of para-/ortho- H_2 molecules by atomic hydrogen on temperature are shown in the left panel of Figure 1. We take into account the transition ortho \rightleftharpoons para using ratio n_{ortho}/n_{para} computed by Flower & Pineau des Forêts (2000) for the temperature range 1 – 10⁴ K. We also estimate the impact of new collisional coefficients by Lique (2015) on the excitation temperatures of rotational transitions of ortho-/para- H_2 and brightness temperatures in the most intensive lines.

The computations of excitation/de-excitation rate coefficients of the lowest ro-vibrational levels of hydrogen deuteride molecules HD by collisions with hydrogen atoms have been done by Flower & Roueff (1999); Roueff & Flower (1999). The complete results for the most transitions with $\Delta J = 1, 2, \dots$ for levels with $J = 0, \dots, 9$ and $v = 0, 1, 2$ are available at the database of VAMDC consortium for the temperature range 100-2080 K with step $\Delta T_K = 20$ K. They are well approximated by cubic polynomials in the log-log scale that is shown in the right panel of Figure 1. The best-fit coefficients are presented in Table 14 in the Appendix of the on-line version. For the temperatures lower 100 K we use the extrapolated values issued by this fit.

The rates of collisional excitation/de-excitation of $u-l$ levels of molecules H_2 and HD (noted as X) are computed as follows

$$C_{ul}^X = \kappa_{ul}^X n_H, \quad C_{lu}^X = \kappa_{lu}^X n_H.$$

In Figure 2 we show the inverse rates collision and radiative excitations, C_{lu}^{-1} and $(B_{lu}U_{\nu_{ul}})^{-1}$, as well as de-excitations, C_{ul}^{-1} and $(B_{ul}U_{\nu_{ul}})^{-1}$, in the halos virialized at different z for comparison with actual age of the Universe t_U and character time of number densities change of molecules, which is estimated as follows $(|d \ln n_X/dt|)^{-1} = (|(z+1)H(z)d \ln n_X/dz|)^{-1}$. Here and below $U_{\nu_{ul}}$ notes the energy density of CMB radiation at the frequency of transition between levels u and l . One can see that in the dark ages halos for molecules H_2 the rates of collisional excitation/de-excitation by atomic hydrogen are comparable with the rates of radiative excitation/de-excitation by CMB quanta. At the high redshifts they are close to the value of rate of spontaneous transition A_{ul} to the base level (Table 2). For molecules HD in the conditions of dark ages halos the rates of collisional excitation/de-excitation are in few order lower than the radiative ones and the rates of spontaneous transitions (Table 2).

³ <https://basecol.vamdc.eu/>

The values presented in Figure 2 also show that for halos formed at $z > 30$ ($T_K > 400$ K, $n_H > 10^6$ m^{-3}) the character times of collisional and radiation excitations/de-excitations of levels 2-5 of H_2 are lower than the age of the Universe and character time of number density change of molecular hydrogen. This means that the population of the rotational levels of molecular hydrogen can be estimated using condition of quasi-stationarity. Later, at $z \leq 30$, when adiabatic temperature of virialized halos is < 400 K the character times of collisional and radiation excitations of levels 2-5 are comparable and higher than the age of the Universe, hence, the condition of quasi-stationarity for populations of the rotational levels there can not be used. For molecules HD this condition can be used for dark ages halos practically always.

The presented here data about rates of spontaneous transitions allowed by quantum selection rules and rates of their collisional de-excitations say us about emission properties of halos in general. For any transition between levels u and l , there is a critical number density of perturbers, n_H^{cr} , at which the radiating molecule suffers collisions at the rate $C_{ul} = A_{ul}$. It means that for $n_H \gg n_H^{cr}$ collisional de-excitations are dominated over spontaneous radiation transitions. In this case the ther-

mal emission in the line vanishes.

One can estimate the critical densities of atomic hydrogen for each level discussed here as $n_H^{cr} = A_{ul}/\kappa_{ul}$. The results of computations are presented in Figure 3. The critical densities for lowest rotational levels of molecular hydrogen H_2 and hydrogen deuteride HD are essentially larger than the density of the atomic hydrogen in the halos. It means that the thermal emission in these lines is expected. The problem is to extract it from the CMB background.

4. POPULATIONS AND EXCITATION TEMPERATURES OF ROTATIONAL LEVELS WITH $J = 0 - 5$

Let's consider the 6-levels system and all collision and radiative transition permitted by the quantum selection rules. Since the conditions of quasi-stationarity in the halos virialized at $z < 30$ are not satisfied for all levels of molecule H_2 the kinetic equations for transitions between levels must be solved. The selection rules for molecule H_2 (electric quadrupole transitions) permit $\Delta J = \pm 2$ for radiative transitions, for molecule HD (electric dipole transitions) they permit $\Delta J = \pm 1$, so the kinetic equations for populations of the rotational levels for these molecules are different.

In the general case before and after virialization the kinetic equations for populations of the rotational levels of H_2 and HD are as follows

H_2 :

$$\begin{aligned} (1+z)H \frac{dX_j}{dz} &= X_j (R_{j,j+2} + C_{j,j+4}) - X_{j+2}R_{j+2,j} - X_{j+4}C_{j+4,j}, \quad j = 0, 1 \\ (1+z)H \frac{dX_j}{dz} &= X_j (R_{j,j-2} + R_{j,j+2}) - X_{j-2}R_{j-2,j} - X_{j+2}R_{j+2,j}, \quad j = 2, 3 \\ (1+z)H \frac{dX_j}{dz} &= X_j (R_{j,j-2} + C_{j,j-4}) - X_{j-2}R_{j-2,j} - X_{j-4}C_{j-4,j}, \quad j = 4, 5 \end{aligned} \quad (1)$$

HD :

$$\begin{aligned} (1+z)H \frac{dY_0}{dz} &= Y_0 \left(R_{01} + \sum_{i=2}^5 C_{0i} \right) - Y_1 R_{10} - \sum_{i=2}^5 Y_i C_{i0}, \\ (1+z)H \frac{dY_j}{dz} &= Y_j \left(R_{j,j-1} + R_{j,j+1} + \sum_{i \neq j, j \pm 1}^5 C_{ji} \right) - Y_{j-1}R_{j-1,j} - Y_{j+1}R_{j+1,j} - \sum_{i \neq j, j \pm 1}^5 Y_i C_{ji}, \quad j = 2, 3, 4 \\ (1+z)H \frac{dY_5}{dz} &= Y_5 \left(R_{54} + \sum_{i=0}^3 C_{5i} \right) - Y_4 R_{45} - \sum_{i=0}^3 Y_i C_{i5}, \end{aligned} \quad (2)$$

where $X_j \equiv n_j/n_{H_2}$ and $Y_j \equiv n_j/n_{HD}$ are fractions of molecular hydrogen and hydrogen deuteride correspondingly in the state with rotational quantum number $J = j$, $R_{ul} = A_{ul} + B_{ul}U_{\nu_{ul}} + C_{ul}$, $R_{lu} = B_{lu}U_{\nu_{ul}} + C_{lu}$. One equation from system (1) for H_2 can be substituted by simple equation

$$\frac{n_1^{H_2} + n_3^{H_2} + n_5^{H_2}}{n_0^{H_2} + n_2^{H_2} + n_4^{H_2}} = \frac{n_{ortho}}{n_{para}}, \quad (3)$$

and one equation from system (2) for HD can be substi-

tuted by

$$n_0^{HD} + n_1^{HD} + n_2^{HD} + n_3^{HD} + n_4^{HD} + n_5^{HD} = n_{HD} \quad (4)$$

after their differentiation with respect to redshift.

We integrate the equations (1)-(2) by the code *ddriv1*⁴ together with equations of evolution of temperature and density of all components as well as with kinetic equations of formation/destruction of molecules in the halo (Novosyadlyj et al. 2018). We set the initial conditions for eqs. (1)-(2) assuming that at $z \geq 200$ the quasi-

⁴ <http://www.netlib.org/slatec/src/ddriv1.f>

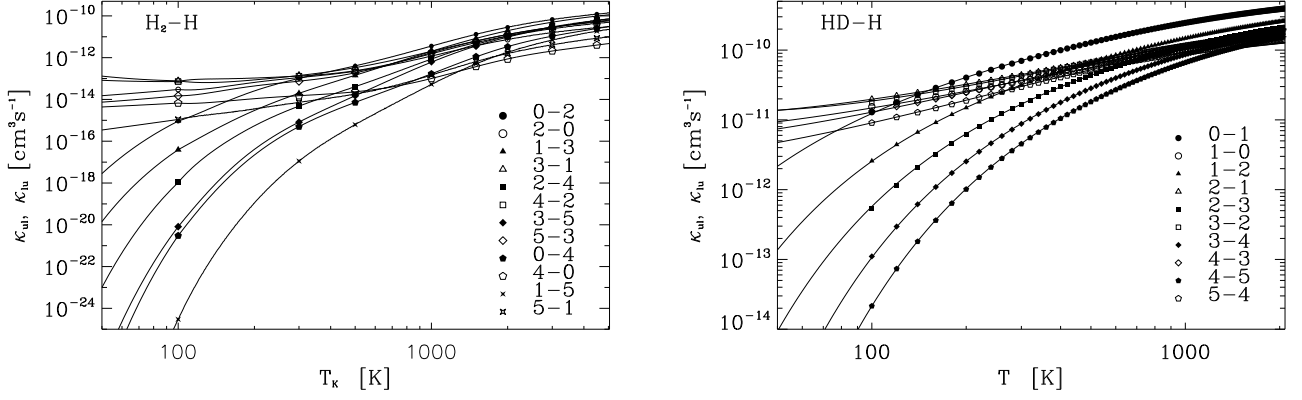


FIG. 1.— Rate coefficients for collisional excitation (κ_{lu} , filled symbols) and de-excitation (κ_{ul} , open symbols) of molecules H₂ and HD by H.

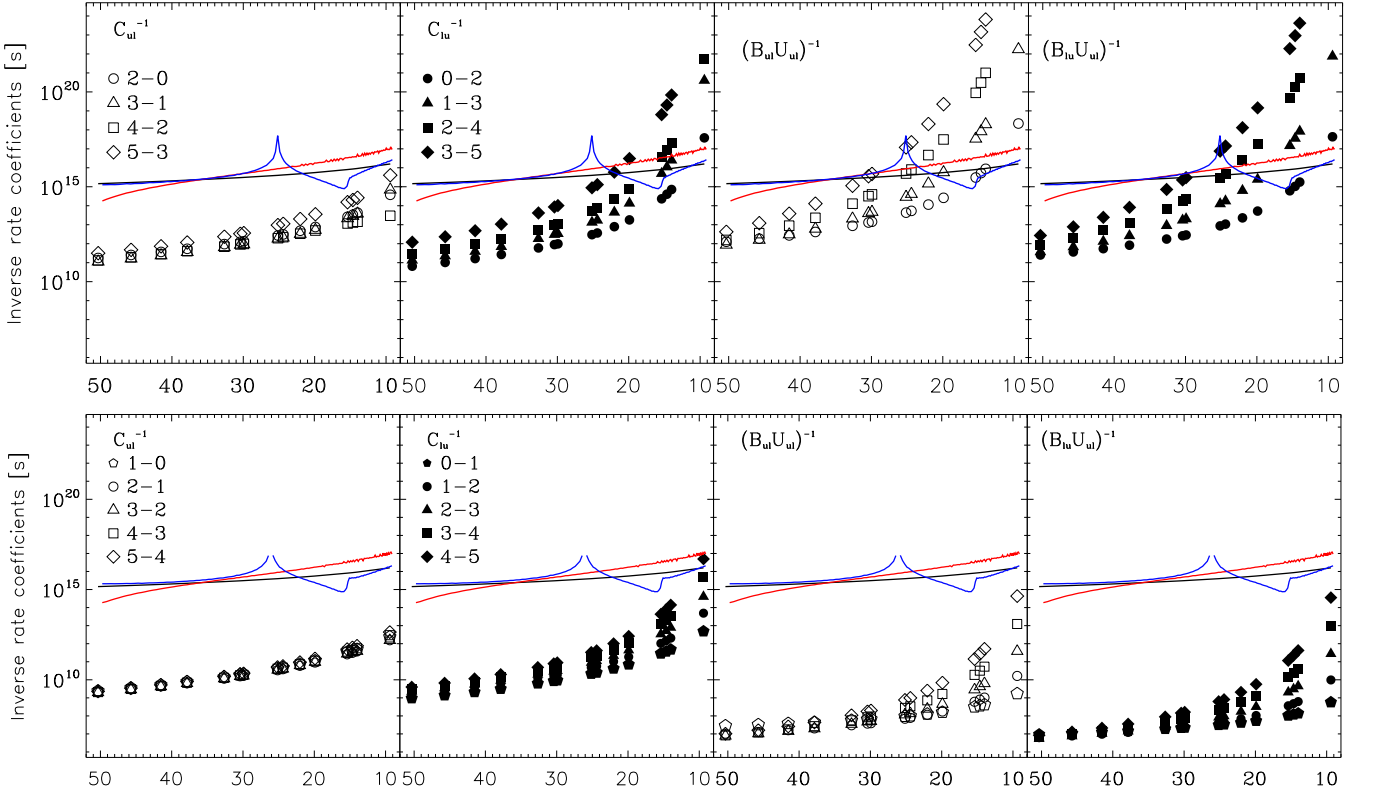


FIG. 2.— The inverse rate coefficients C_{ul}^{-1} , C_{lu}^{-1} , $(B_{ul}U_{\nu_{ul}})^{-1}$ and $(B_{lu}U_{\nu_{lu}})^{-1}$ for molecules H₂ (top panel) and HD (bottom panel) in halos virialized at different z . The black solid line shows the age of the Universe corresponding to z , the red solid line shows the characteristic time of number density change of molecules H₂/HD in halo virialized at $z \approx 50$ and blue line at $z \approx 15$.

stationary condition is satisfied and we solve the system of algebraic equations for H₂ and HD separately. In such way we obtain the evolution of populations of the rotational levels, opacities and the line intensities at all stages formation and existence of dark ages halos.

Dark ages halos after virialization have unchanged density, temperature and chemical composition, hence, the conditions of stationarity of populations of energy levels are satisfied for them. In this case the left parts of eqs. (1)-(2) are zero,

$$\frac{dX_j}{dz} = 0, \quad \frac{dY_j}{dz} = 0,$$

and we have two systems of algebraic equations (1) and (2) which can be solved by standard methods if their last equations, for example, will be substituted by equations (3)-(4) correspondingly. We use for that the subroutine `dgesv.f` from `lapack` library.

When the populations of the rotational levels are computed, we can calculate the excitation temperatures for $l - u$ levels:

$$T_{ex} = \frac{h\nu_{ul}}{k_B} \left[\ln \frac{g_u n_l}{g_l n_u} \right]^{-1}.$$

They are presented for for $l - u$ levels of molecules H₂

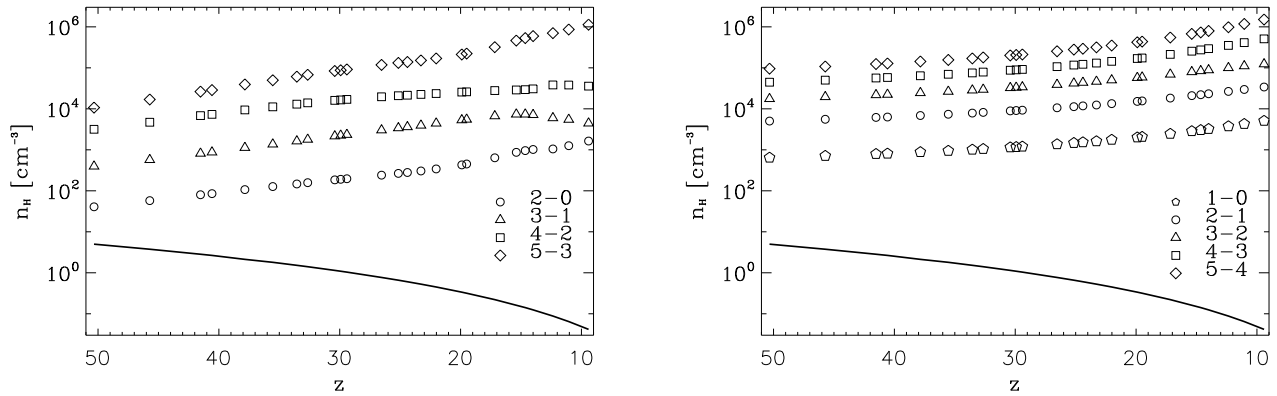


FIG. 3.— The critical number density for lowest energy levels of molecular hydrogen (left panel) and hydrogen deuteride (right panel) in the dark ages halos virialized at different redshifts. The solid line shows the real values of number density of molecular hydrogen in the halos virialized at z .

TABLE 3

THE EXCITATION TEMPERATURES FOR LOWEST ROTATIONAL LEVELS OF H_2 -MOLECULES IN THE HALOS FORMED AT THE REDSHIFTS $z = 30 - 10$.

z	T_K [K]	T_R [K]	T_{ex} [K]			
			0-2	1-3	2-4	3-5
30.41	402.1	85.6	93.7	93.3	113.4	145.7
25.15	298.9	71.3	76.1	77.5	102.9	130.3
19.90	206.3	57.0	59.7	62.7	89.5	108.6
14.65	124.3	42.7	43.8	48.1	69.9	79.4
9.41	59.8	28.4	28.8	32.9	43.7	44.6

TABLE 4

THE EXCITATION TEMPERATURES FOR LOWEST ROTATIONAL LEVELS OF MOLECULES HD IN THE HALOS FORMED AT THE REDSHIFTS $z = 30 - 10$.

z	T_K [K]	T_R [K]	T_{ex} [K]			
			0-1	1-2	2-3	3-4
30.41	402.1	85.61	85.71	85.64	85.63	85.63
25.15	298.9	71.27	71.32	71.29	71.28	71.28
19.90	206.3	56.96	56.98	56.97	56.97	56.97
14.65	124.3	42.65	42.66	42.66	42.66	42.66
9.41	59.8	28.37	28.37	28.37	28.37	28.37

and HD in Tables 3 and 4 accordingly for the dark ages halos with mass $M_h = 5.3 \cdot 10^9 M_\odot$ and different initial amplitude of matter density perturbations, which are virialized at $z = 30.41, 25.15, 19.90, 14.65$ and 9.41 . The kinetic temperature of gas in halos and CMB temperature are presented for comparison. One can see that values of $T_{ex} - T_R > 0$, so, the halos are warmer spots in the cosmic microwave background. Note, that these values are essentially larger for molecules H_2 than for HD. It is because the hydrogen deuteride molecule are asymmetrical, has nonzero electric dipole moment and more effectively interacts with radiation. The data in Table 2 and in Figure 2 support this explanation.

The excitation temperatures of the lowest rotational

levels of molecular hydrogen are sensitive to the ratio of n_{ortho}/n_{para} and values of rate coefficients of their collisional excitation/de-excitation by atomic hydrogen. We re-compute the transitions ortho \rightleftharpoons para and populations of the rotational levels using the rate coefficients revised by Lique (2015). It resulted in some differences with the data of Flower & Pineau des Forêts (2000): in the temperature range 1000-10 K, the ratio n_{ortho}/n_{para} changes in the range 1-1.3, instead of 2.8-0.3. The excitation temperatures, however, do not change so radically: differences do not exceed 4% for the first excited levels of para- and ortho- H_2 with $J = 2$ and $J = 3$ accordingly. But the populations of these levels changed more significantly: in the temperature range of ~ 400 -60 K the population of the first excited level of para- H_2 increases by 1.7-2.2 times, while the population of the first excited level of ortho- H_2 decreases by 1.6-3.2 times.

5. OPACITY AND BRIGHTNESS TEMPERATURE OF DARK AGES HALOS IN ROTATIONAL LINES OF MOLECULES H_2 AND HD

The opacity at the frequency of $u - l$ transition is calculated in the rest frame of the halo as

$$\tau_{ul} = \int_0^{r_h} \alpha_{\nu_{ul}}(r) dr,$$

where $\alpha_{\nu_{ul}}$ is the absorption coefficient per unit of length in frequency ν_{ul} , and r_h is radius of halo.

The absorption coefficient per unit of length in frequency ν_{ul} is as follows (formulas (2.69) and (2.154) in Lang (1974)):

$$\alpha_{\nu_{ul}} = \frac{c^2}{8\pi\nu_{ul}^2} \frac{n_l}{\Delta\nu_L} \frac{g_u}{g_l} \left[1 - \exp\left(-\frac{h\nu_{ul}}{k_B T_{ex}}\right) \right] A_{ul}, \quad (5)$$

where n_l is the number density of molecules in the lower level l , k_B is Boltzmann constant, A_{ul} is the spontaneous transition probability (Einstein coefficient), T_{ex} is excitation temperature for $u - l$ transition, $\Delta\nu_L$ is the width of line at a half-maximum. The last value in the case of the virialized halo can be presented like in the case of turnaround halo (Maoli et al. 1996):

$$\frac{\Delta\nu_L}{\nu} = \frac{2}{c} \sqrt{\frac{2 \ln 2 k_B T_K}{m}} = 7.16 \cdot 10^{-7} \sqrt{\frac{T_K}{m_A}}, \quad (6)$$

where T_K is kinetic temperature (adiabatic or virial) of gas in halo, m and m_A are atomic mass and atomic number of a molecule correspondingly. In the visible center of the spherical homogeneous top-hat halo the optical depth in rotational line ν_{ul} is as follows

$$\tau_{ul} = 1.55 \cdot 10^{50} n_l \frac{g_u}{g_l} \frac{A_{ul}}{\nu_{ul}^3} \sqrt{\frac{m_A}{T_k}} \left[1 - \exp\left(-\frac{h\nu_{ul}}{k_B T_{ex}}\right) \right] r_h, \quad (7)$$

where r_h is its radius in units of Mpc (the rest values must be in CGS system).

TABLE 5
THE OPACITY OF HALOS WITH $M_h = 5.3 \cdot 10^9 M_\odot$ VIRIALIZED AT DIFFERENT REDSHIFTS z_v IN THE LOWEST ROTATIONAL LEVELS OF MOLECULAR HYDROGEN H₂.

z_v	τ_{ul}			
	2-0	3-1	4-2	5-3
30.41	$8.67 \cdot 10^{-9}$	$4.24 \cdot 10^{-8}$	$5.23 \cdot 10^{-10}$	$2.94 \cdot 10^{-11}$
25.15	$4.99 \cdot 10^{-9}$	$2.48 \cdot 10^{-8}$	$8.55 \cdot 10^{-11}$	$2.74 \cdot 10^{-12}$
19.90	$2.67 \cdot 10^{-9}$	$1.35 \cdot 10^{-8}$	$7.26 \cdot 10^{-12}$	$1.13 \cdot 10^{-13}$
14.65	$1.43 \cdot 10^{-9}$	$6.64 \cdot 10^{-9}$	$1.76 \cdot 10^{-13}$	$9.45 \cdot 10^{-16}$
9.41	$9.40 \cdot 10^{-10}$	$2.60 \cdot 10^{-9}$	$2.72 \cdot 10^{-16}$	$1.09 \cdot 10^{-19}$

TABLE 6
THE OPACITY OF HALOS WITH $M_h = 5.3 \cdot 10^9 M_\odot$ VIRIALIZED AT DIFFERENT REDSHIFTS z_v IN THE LOWEST ROTATIONAL LEVELS OF HYDROGEN DEUTERIDE MOLECULES HD.

z_v	τ_{ul}			
	1-0	2-1	3-2	4-3
30.41	$2.25 \cdot 10^{-7}$	$1.23 \cdot 10^{-7}$	$9.69 \cdot 10^{-9}$	$1.51 \cdot 10^{-10}$
25.15	$3.17 \cdot 10^{-7}$	$1.22 \cdot 10^{-7}$	$5.18 \cdot 10^{-9}$	$3.28 \cdot 10^{-11}$
19.90	$4.28 \cdot 10^{-7}$	$9.93 \cdot 10^{-8}$	$1.69 \cdot 10^{-9}$	$2.78 \cdot 10^{-12}$
14.65	$3.12 \cdot 10^{-7}$	$3.23 \cdot 10^{-8}$	$1.21 \cdot 10^{-10}$	$2.09 \cdot 10^{-14}$
9.41	$1.25 \cdot 10^{-7}$	$2.74 \cdot 10^{-9}$	$4.98 \cdot 10^{-13}$	$9.58 \cdot 10^{-19}$

The results of computations of τ_{ul} for the lowest rotational levels of molecules para-/ortho-H₂ and HD are presented in Tables 5 and 6 accordingly. The opacities in the frequency ν_{31} of ortho-H₂ molecule is larger than in the frequency ν_{20} of para-H₂ molecule because $n_{ortho}/n_{para} \approx 3$ (Flower & Pineau des Forêts 2000). They decrease with decreasing of z_v because the number density of molecules decreases (Table 1) as well as the populations of non-base levels of both molecules via decreasing of excitation temperatures (Table 3 and 4). The opacity related with the base level of HD molecule is not monotonic function of z_v (2nd column of Table 6) since its population ($n_{J=0}/n_{HD}$) fast increases with decreasing of excitation temperature.

We note also, that opacities of the dark ages halos in the rotational lines of molecule HD are higher than in the lines of H₂ in spite of the $n_{HD}/n_{H_2} \sim 10^{-4}$. It has simple explanation: the factor A_{ul}/ν_{ul}^2 in (5) is essentially larger for HD than for H₂.

We also have analyzed the evolution of opacities of single halos during its formation. The results for the

brightest lines of H₂ and HD molecules for halos with mass $M_h = 5.3 \cdot 10^9 M_\odot$ and different initial amplitudes of density perturbation are presented in the left panels of Figures 4 and 5 accordingly. The same results for other lines and other halos are presented in the animate figures 8 and 9 in Appendix of the on-line version. One can see that halos formed earlier have larger opacity at lower redshifts, in comparison with halos formed at the same redshifts, since they are denser.

The differential brightness temperature for thermal emission is obtained from the radiative transfer equation and is as follows

$$\delta T_{ul}^b = \frac{h\nu_{obs}}{k_B} \left[\frac{1}{e^{\frac{h\nu_{ul}}{k_B T_{ex}}} - 1} - \frac{1}{e^{\frac{h\nu_{ul}}{k_B T_R}} - 1} \right] (1 - e^{-\tau_{ul}}),$$

where T_b is the Rayleigh-Jeans brightness temperature, T_{ex} is the excitation temperature of a transition $u-l$ and T_R is temperature of the background radiation. The dark ages halos are optically thin in the molecular lines, so, $(1 - e^{-\tau_{ul}}) \approx \tau_{ul}$, and the expression for the brightness temperature of thermal emission of dark ages halos becomes as follows

$$\delta T_{ul}^b = \frac{7.44 \cdot 10^{39} n_u A_{ul}}{(1+z)\nu_{ul}^2} \sqrt{\frac{m_A}{T_K}} \left[\frac{e^{\frac{h\nu_{ul}}{k_B T_R}} - e^{\frac{h\nu_{ul}}{k_B T_{ex}}}}{e^{\frac{h\nu_{ul}}{k_B T_R}} - 1} \right] \frac{r_h}{1 \text{ Mpc}}, \quad (8)$$

where n_u is in units cm^{-3} . Since the observable differential brightness temperature is not homogeneous in the surface of halo we can average it like

$$\langle \delta T_{br} \rangle = 2 \int_0^1 \delta T_{br}(x) x dx,$$

where $x = \theta/\theta_h$. In our case the integral has exact analytical presentation which for small values of τ_{ul} gives factor $2/3$:

$$\langle \delta T_{ul}^b \rangle = \frac{2}{3} \delta T_{ul}^b. \quad (9)$$

The expression (8) gives us the possibility to understand when thermal emission signal from dark ages halos can be sighted in the cosmic microwave background. For that the additional perturbers are necessary in order $T_{ex} > T_R$. If $T_{ex} \rightarrow T_R$ then $\delta T_{ul}^b \rightarrow 0$. The halos should be dense and extended to have large opacities. The emitting molecules must be abundant and have a large value of ratio of Einstein coefficients to square frequency for excited levels. The maximal value of differential brightness temperature is expected in the case when $T_{ex} \gg h\nu_{ul}/k_B$ and value in brackets in (8) is close to 1.

We use the data from Tables 1, 11 and 2 for computation the differential brightness temperatures in the lowest rotational frequencies of molecules H₂ and HD for halos formed at $z = 10 - 50$. The results for halos with $M_h = 5.3 \cdot 10^9 M_\odot$ are presented in Tables 7 and 8 for molecules H₂ and HD accordingly. First of all we note that thermal emission of dark ages halos in the low rotational level of molecules H₂ and HD exist but the value of differential brightness temperatures are too low to be detected by current instrumentation. They are larger for halos virialized earlier and vanishes for halos virialized late.

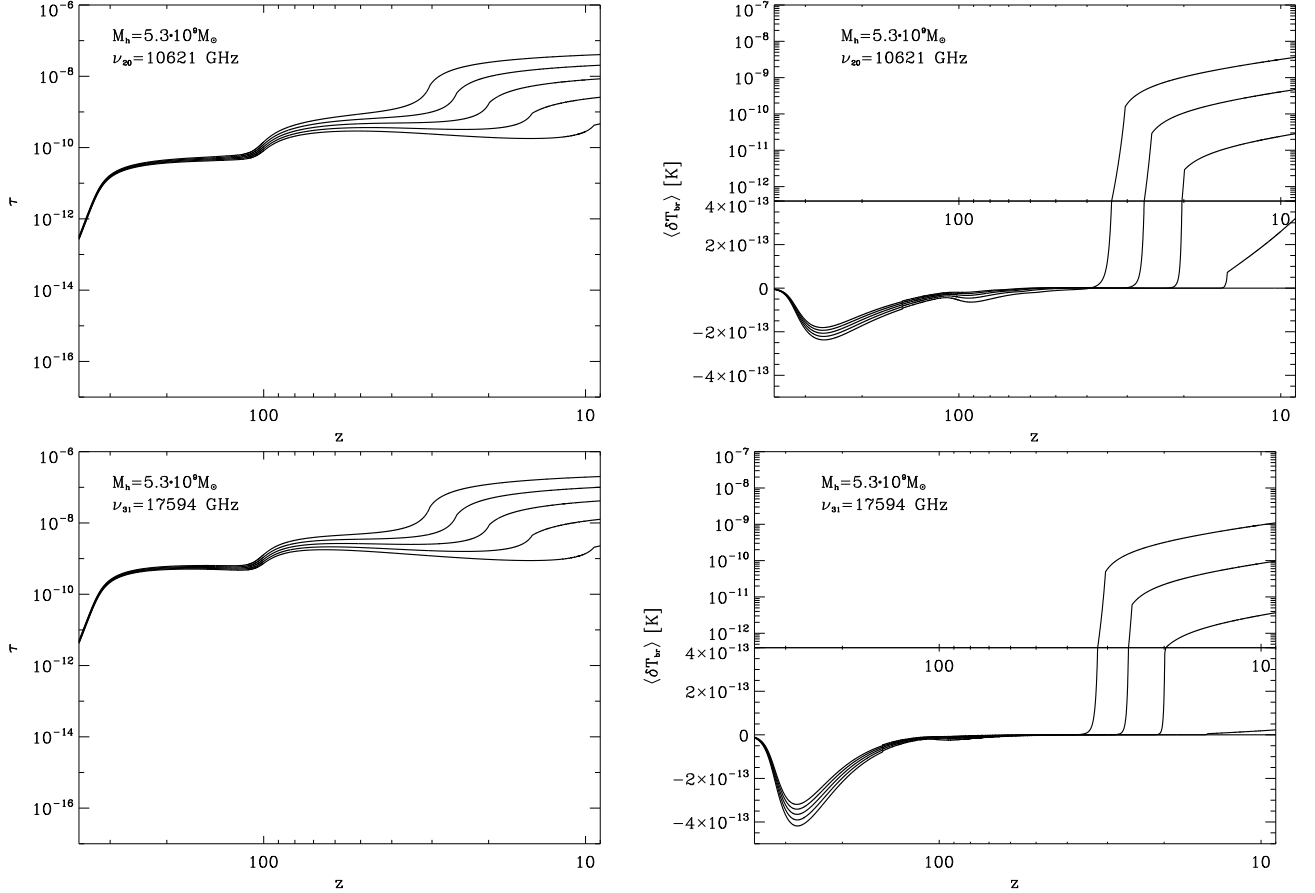


FIG. 4.— Evolution of opacity (left column) and brightness temperature (right column) in the lines of transitions $J = 2 \rightarrow 0$ (top row) and $J = 3 \rightarrow 1$ (bottom row) of molecule H_2 for halos with mass $M_h = 5.3 \cdot 10^9 M_\odot$. Each line corresponds to the halo with different initial amplitude of curvature perturbation: $C_k = 3 \cdot 10^{-4}$, $2.5 \cdot 10^{-4}$, $2 \cdot 10^{-4}$, $1.5 \cdot 10^{-4}$, $1 \cdot 10^{-4}$ (from top to bottom in the right hand side of each panel).

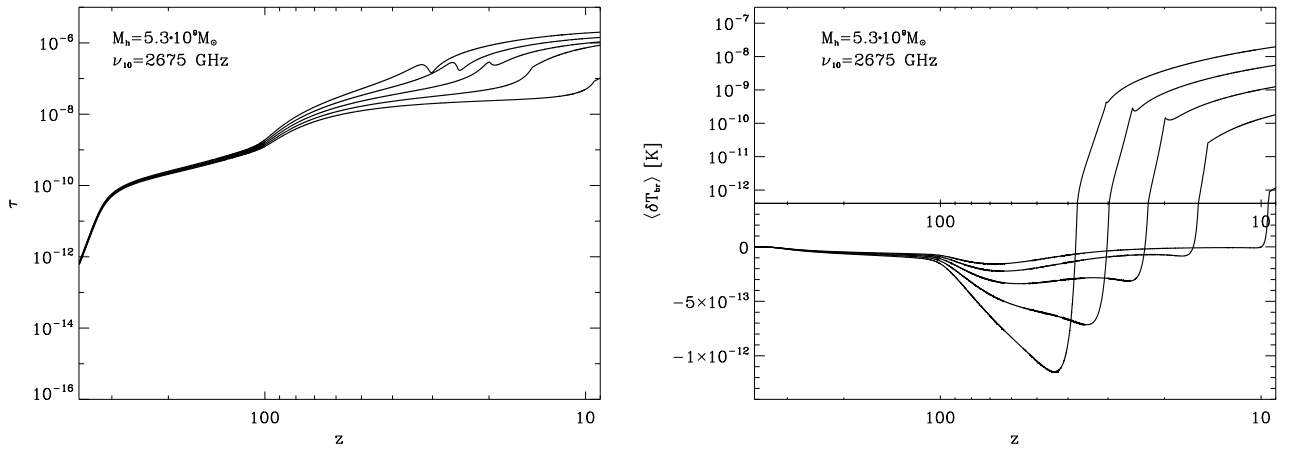


FIG. 5.— Evolution of opacity (left column) and brightness temperature (right column) in the lines of transitions $J = 1 \rightarrow 0$ of molecule HD for halos with mass $M_h = 5.3 \cdot 10^9 M_\odot$. Each line corresponds to the halo with different initial amplitude of curvature perturbation as in the previous figure.

We also have analyzed the evolution of differential brightness temperature in the rotational lines of H_2 and HD of single halos during its formation. The results are shown for the lowest transitions ($J = 2 \rightarrow 0$ / $J = 3 \rightarrow 1$ for para-/ortho- H_2 and $J = 1 \rightarrow 0$ HD molecules) in the right panels of Figures 4 and 5 for halos with mass $M_h = 5.3 \cdot 10^9 M_\odot$ and for other transitions and halos of other mass are presented in the animate figures 8 and 9 in

Appendix of the on-line version. These figures are combination of logarithmic and normal scales since before the turn around of halos and even some time of the beginning of the collapse the differential brightness temperature are negative since $T_{ex} < T_R$ because the adiabatic temperature of gas is lower than CMB temperature, $T_K < T_R$. In the case of molecule HD we see the deep lowering of the brightness temperature for transition $J = 1 \rightarrow 0$,

TABLE 7

THERMAL EMISSION: THE DIFFERENTIAL BRIGHTNESS TEMPERATURES OF HALOS WITH $M_h = 5.3 \cdot 10^9 M_\odot$ VIRIALIZED AT DIFFERENT REDSHIFTS z_v IN THE LOWEST ROTATIONAL LEVELS OF MOLECULAR HYDROGEN H₂.

z_v	$\langle \delta T_{ul}^b \rangle$ [K]			
	2-0	3-1	4-2	5-3
30.41	$1.64 \cdot 10^{-10}$	$4.92 \cdot 10^{-11}$	$4.08 \cdot 10^{-13}$	$3.40 \cdot 10^{-14}$
25.15	$2.92 \cdot 10^{-11}$	$6.13 \cdot 10^{-12}$	$2.87 \cdot 10^{-14}$	$1.12 \cdot 10^{-15}$
19.90	$2.87 \cdot 10^{-12}$	$3.82 \cdot 10^{-13}$	$5.61 \cdot 10^{-16}$	$6.03 \cdot 10^{-18}$
14.65	$7.57 \cdot 10^{-14}$	$5.13 \cdot 10^{-15}$	$4.63 \cdot 10^{-19}$	$4.33 \cdot 10^{-22}$
9.41	$1.55 \cdot 10^{-16}$	$9.80 \cdot 10^{-19}$	$4.53 \cdot 10^{-26}$	$3.39 \cdot 10^{-32}$

TABLE 8

THERMAL EMISSION: THE DIFFERENTIAL BRIGHTNESS TEMPERATURES OF HALOS WITH $M_h = 5.3 \cdot 10^9 M_\odot$ VIRIALIZED AT DIFFERENT REDSHIFTS z_v IN THE LOWEST ROTATIONAL LEVELS OF HYDROGEN DEUTERIDE MOLECULES HD.

z_v	$\langle \delta T_{ul}^b \rangle$ [K]			
	1-0	2-1	3-2	4-3
30.41	$4.28 \cdot 10^{-10}$	$5.32 \cdot 10^{-11}$	$2.02 \cdot 10^{-12}$	$3.68 \cdot 10^{-14}$
25.15	$2.84 \cdot 10^{-10}$	$2.29 \cdot 10^{-11}$	$4.66 \cdot 10^{-13}$	$4.50 \cdot 10^{-15}$
19.90	$1.45 \cdot 10^{-10}$	$6.08 \cdot 10^{-12}$	$4.94 \cdot 10^{-14}$	$2.00 \cdot 10^{-16}$
14.65	$2.59 \cdot 10^{-11}$	$3.44 \cdot 10^{-13}$	$5.98 \cdot 10^{-16}$	$6.11 \cdot 10^{-19}$
9.41	$9.01 \cdot 10^{-13}$	$9.67 \cdot 10^{-16}$	$6.33 \cdot 10^{-20}$	$3.60 \cdot 10^{-24}$

slight decrease for transition $J = 2 \rightarrow 1$ and its absence for transitions between upper levels before appearance of emission. Their amplitudes, however, are too small to discuss the possibility of their observations.

Another measure of the halo signal extracted from the cosmic background radiation is the differential energy flux per unit frequency (Iliev et al. 2002)

$$\begin{aligned}
 \delta F_{ul} &= \frac{2\pi}{c} \left(\frac{\nu_{ul}}{1+z} \right)^2 k_B \langle \delta T_{ul}^b \rangle \theta_h^2 \\
 &= \frac{2.27}{(1+z)^2} \left(\frac{\nu_{ul}}{1 \text{ GHz}} \right)^2 \left(\frac{\langle \delta T_{ul}^b \rangle}{1 \text{ K}} \right) \left(\frac{\theta_h}{1''} \right)^2 \mu\text{Jy}
 \end{aligned} \quad (10)$$

For the values of differential brightness temperatures presented in Tables 7 and 8 the values of differential energy flux $\delta F_{ul} \leq 10^{-5} \mu\text{Jy}$. In Tables 15 and 16 we present them for the rest halos and two lowest transitions of molecules H₂ and HD accordingly. The maximal values of differential energy fluxes we obtain for halo of maximal mass ($M_h = 5.3 \cdot 10^9 M_\odot$) which virialized earliest ($z_v = 30.41$). For example, in the frequency 338 GHz (transition $J = 2 \rightarrow 0$ of para-H₂ molecule) it is $\sim 4 \cdot 10^{-5} \mu\text{Jy}$. The maximal flux in the frequency 85 GHz ($J = 1 \rightarrow 0$) of the molecule HD is estimated as $\sim 7 \cdot 10^{-6} \mu\text{Jy}$. Both values are essentially lower of the sensitivity of current radio telescopes.

One can conclude that so small value of expected molecular hydrogen emission from dark ages halos are caused by low values of adiabatic temperature in them. Really, the virialization temperature of halos can be essentially larger than adiabatic temperature caused by smooth homogeneous collapse (Barkana et al. 2001; Bromm & Yoshida 2011; Novosyadlyj et al. 2018). Local

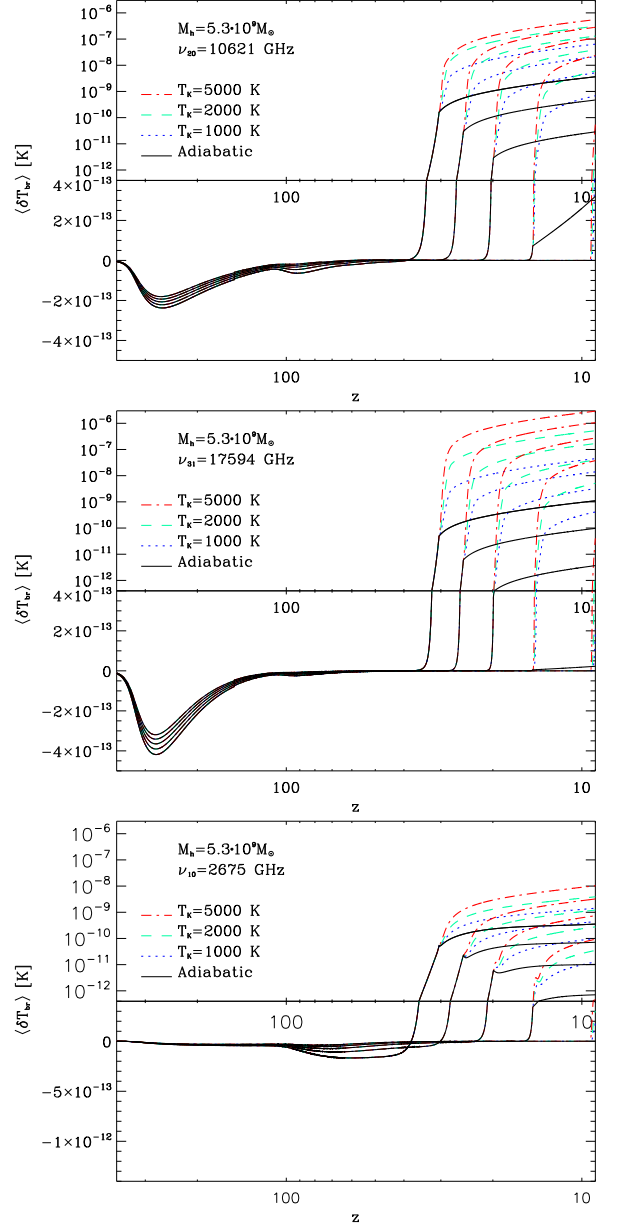


FIG. 6.— Evolution of brightness temperature in the lines of transitions $J = 2 \rightarrow 0$ and $J = 3 \rightarrow 1$ of molecule H₂ and $J = 1 \rightarrow 0$ of molecule HD for halos with mass $M_h = 5.3 \cdot 10^9 M_\odot$. Each line corresponds to the halo with different initial amplitude of curvature perturbation like in previous figures and different final temperature.

inhomogeneities, shock waves, fragmentation and other nonlinear phenomena will enhance the kinetic temperature of gas in halos. Let's estimate the differential brightness temperature of dark ages halos in the rotational lines of hydrogen molecules for higher kinetic temperatures of gas in the virialized halos which had the same history before. We suppose that halos after virialization reach some temperatures $T_{K(vir)} > T_{K(ad)}$ independent on the redshift of virialization. The results for $T_{K(vir)} = 1000, 2000, 5000$ K are presented in Figure 6. Really, increasing of kinetic temperature of gas in the virialized halos leads to the increasing of their differential brightness temperature in the rotational lines of molecular hydrogen. We see that for para/ortho-hydrogen molecules the effect of tem-

perature is larger than for hydrogen deuteride ones, and the base line of ortho-H₂ is more intensive than para-H₂. The values of the differential brightness temperatures of hot halos ($T_{K(vir)} \gtrsim 2000$ K) are comparable with the sensitivity of Planck observatory (Planck Collaboration 2018a) and expected sensitivity of SKA radio telescope that is being built, $\langle \delta T_{ul}^b \rangle \sim 10^{-6}$ K. Both, unfortunately, are far from the angular resolution which is necessary to detect individual halos analyzed here.

It is interesting to compare our results with estimations of H₂ and HD emission in the same lines from the primordial object, either Pop III galaxies or primordial clouds, which have been computed and discussed by Kamaya & Silk (2002, 2003); Omukai & Kitayama (2003); Mizusawa et al. (2005). The expected emission flux from the molecular cloud cores at the redshift of $z \sim 20$ in the $J = 2 \rightarrow 0$ line of H₂ is $\sim 2 \cdot 10^{-7}$ Jy, and in the $J = 4 \rightarrow 3$ line of HD is $\sim 8 \cdot 10^{-9}$ Jy (Kamaya & Silk 2003). The differential spectral fluxes δF in these lines at $z \sim 24$ from the smallest halos analyzed here are $3 \cdot 10^{-15}$ and $3 \cdot 10^{-19}$ Jy accordingly. Since the differential brightness temperature δT_{br} in those lines are $1.5 \cdot 10^{-12}$ K and $1.9 \cdot 10^{-16}$ K respectively, and $\delta F \propto \delta T_{br}$, and $F \propto T_{br}$ with the same coefficient of proportion, the spectral fluxes in these lines are $\sim 5 \cdot 10^{-3}$ Jy. Omukai & Kitayama (2003) have estimated the energy fluxes in the rotational lines of H₂ molecule from forming galaxies at $z = 20$: $8 \cdot 10^{-27}$ erg/cm²s ($J = 2 \rightarrow 0$) and $5.6 \cdot 10^{-26}$ erg/cm²s ($J = 3 \rightarrow 1$) for galaxies with $M = 10^7 M_\odot$, and $9 \cdot 10^{-24}$ erg/cm²s ($J = 2 \rightarrow 0$) and $7.7 \cdot 10^{-23}$ erg/cm²s ($J = 3 \rightarrow 1$) for galaxies with $M = 10^9 M_\odot$. According to our results (Table 15 in Appendix), the fluxes in these lines are as follows: $8 \cdot 10^{-22}$ erg/cm²s ($J = 2 \rightarrow 0$) and $3.6 \cdot 10^{-21}$ erg/cm²s ($J = 3 \rightarrow 1$) for galaxies with $M = 10^7 M_\odot$, and $7 \cdot 10^{-20}$ erg/cm²s ($J = 2 \rightarrow 0$) and $3.2 \cdot 10^{-19}$ erg/cm²s ($J = 3 \rightarrow 1$) for galaxies with $M = 5.3 \cdot 10^9 M_\odot$. So, fluxes in lower rotational lines of hydrogen and hydrogen deuteride molecules from dark ages halos analyzed here are in ~ 4 order higher than the fluxes in the same lines from other primordial objects. Such large difference is caused mainly by the difference in structural models of sources and the mechanisms of excitation/de-excitation of the rotational levels. In our case the excitation by CMB is dominant, but in foregoing studies the thermal luminescence has been analyzed.

We estimate also how the predictions of opacities of halos and brightness temperatures in the lines of transitions between rotational levels of ortho-/para-H₂ change with collision rate coefficients revised by Lique (2015). In the line of transition $J = 0 \rightarrow 2$ (para-H₂) the opacities increase by 1.2-1.8 times for the halos virialized at $z=30-10$, while in the line of transition $J = 1 \rightarrow 3$ (ortho-H₂) the opacities decrease by 1.1-1.7 times. These differences as well as the change the populations of levels and excitation temperatures lead to change the differential brightness temperature. In the halos with kinetic temperature $\gtrsim 170$ K the differential brightness temperature in the base line of para-H₂ ($J = 2 \rightarrow 0$) increases by 1.4-1.7 times, for colder halos it increases by 3.5-5.4 times. While, the base line of ortho-H₂ ($J = 3 \rightarrow 1$), vice versa, decreases by 1.7-2.6 times for warmer halos

and decreases ~ 3.5 times for colder ones. Hence, the main conclusion of this re-analysis is that revised collisional excitation/de-excitation coefficients do not change the main results and conclusions.

6. RESONANT SCATTERING

The resonant scattering of CMB quanta in the rotational lines of molecules in the dark ages halo which has optical depth τ_{ul} and peculiar velocity v_p leads to differential brightness temperature (Maoli et al. 1996; Persson et al. 2010)

$$\delta T_{ul}^b = \frac{h^2 \nu_{ul}^2}{k_B^2 T_R} \frac{\tau_{ul}}{\left(1 - e^{-\frac{h\nu_{ul}}{k_B T_R}}\right)^2} \frac{v_p}{c} \cos \theta, \quad (11)$$

where θ is the angle between the vector of peculiar velocity and the line of sight of the terrestrial observer. The rms value of peculiar velocity averaged over spherical region with radius R can be estimated if the power spectrum $P(k; z)$ of initial density perturbations is known

$$\langle v_p^2 \rangle = \frac{H^2(z)}{2\pi^2(1+z)^2} \int_0^\infty P(k; z) W^2(kR) dk, \quad (12)$$

where $W(x) \equiv 3(\sin x - x \cos x)/x^3$ is the top-hat sphere in Fourier space. We present the $V_{rms} \equiv \langle v_p^2 \rangle^{1/2}$ as function of smoothing scale R for power spectrum of Λ CDM model with post-Planck cosmological parameters (Planck Collaboration 2018a; Planck collaboration 2018b) in Figure 7. The power spectrum $P(k; z) \equiv A_s(z) k^{n_s} T^2(k; z)$ we have normalized by computation of $\sigma_8 = 0.806$ for the current epoch using the fitting formula for the transfer function $T(k; z)$ proposed by Eisenstein & Hu (1998). We rescaled the amplitude $A_s(z)$ for different redshifts using the square of the growth function $D(z)$ by Carroll et al. (1998).

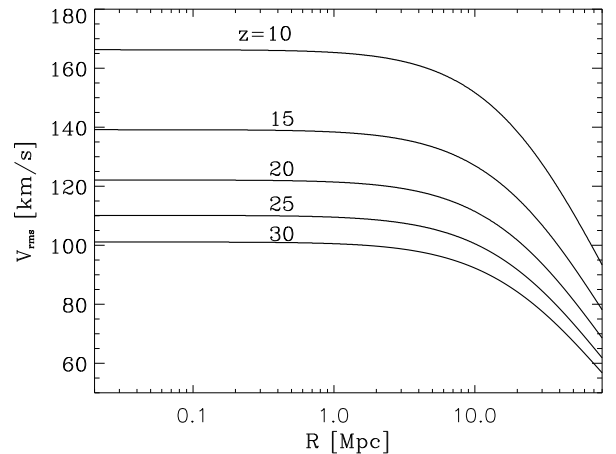


FIG. 7.— The rms peculiar velocity averaged in the top-hat sphere with radius R at different redshifts in the Λ CDM model with post-Planck cosmological parameters (Planck collaboration 2018b).

We compute the absolute values of differential brightness temperature δT_{ul}^b and spectral flux δF_{ul} caused by resonant scattering in the same rotational lines of para-H₂, ortho-H₂ and HD molecules for the same halos. The

TABLE 9

RESONANT SCATTERING: THE DIFFERENTIAL BRIGHTNESS TEMPERATURES OF HALOS WITH $M_h = 5.3 \cdot 10^9 M_\odot$ VIRIALIZED AT DIFFERENT REDSHIFTS z_v IN THE LOWEST ROTATIONAL LEVELS OF MOLECULAR HYDROGEN H₂.

z_v	$\langle \delta T_{ul}^b \rangle$ [K]			
	2-0	3-1	4-2	5-3
30.41	$1.53 \cdot 10^{-11}$	$4.11 \cdot 10^{-12}$	$2.13 \cdot 10^{-15}$	$4.78 \cdot 10^{-18}$
25.15	$3.49 \cdot 10^{-12}$	$4.34 \cdot 10^{-13}$	$2.92 \cdot 10^{-17}$	$1.77 \cdot 10^{-20}$
19.90	$4.31 \cdot 10^{-13}$	$1.68 \cdot 10^{-14}$	$5.57 \cdot 10^{-20}$	$5.39 \cdot 10^{-24}$
14.65	$1.75 \cdot 10^{-14}$	$8.77 \cdot 10^{-17}$	$2.09 \cdot 10^{-24}$	$1.08 \cdot 10^{-29}$
9.41	$5.15 \cdot 10^{-17}$	$2.95 \cdot 10^{-21}$	$5.83 \cdot 10^{-33}$	$5.36 \cdot 10^{-41}$

TABLE 10

RESONANT SCATTERING: THE DIFFERENTIAL BRIGHTNESS TEMPERATURES OF HALOS WITH $M_h = 5.3 \cdot 10^9 M_\odot$ VIRIALIZED AT DIFFERENT REDSHIFTS z_v IN THE LOWEST ROTATIONAL LEVELS OF HYDROGEN DEUTERIDE MOLECULES HD.

z_v	$\langle \delta T_{ul}^b \rangle$ [K]			
	1-0	2-1	3-2	4-3
30.41	$3.57 \cdot 10^{-9}$	$1.17 \cdot 10^{-9}$	$4.37 \cdot 10^{-11}$	$2.77 \cdot 10^{-13}$
25.15	$4.24 \cdot 10^{-9}$	$7.98 \cdot 10^{-10}$	$1.23 \cdot 10^{-11}$	$2.41 \cdot 10^{-14}$
19.90	$4.42 \cdot 10^{-9}$	$3.56 \cdot 10^{-10}$	$1.45 \cdot 10^{-12}$	$4.80 \cdot 10^{-16}$
14.65	$2.06 \cdot 10^{-9}$	$3.86 \cdot 10^{-11}$	$1.68 \cdot 10^{-14}$	$2.84 \cdot 10^{-19}$
9.41	$3.05 \cdot 10^{-10}$	$2.90 \cdot 10^{-13}$	$1.40 \cdot 10^{-18}$	$6.13 \cdot 10^{-26}$

results are presented in Tables 9-10 and Tables 15-16 in Appendix of the on-line version of the paper. They show that expected amplitudes of intensities of emission/absorption in the rotational lines of both isomers of molecular hydrogen caused by resonant scattering are by order and more lower than caused by thermal collisions with adiabatically warmed gas in the dark ages halos. And contrary, the amplitudes of halo intensities in the rotational lines of HD molecule caused by resonant scattering are systematically higher than thermal emission intensities. The effect is more noticeable at small redshifts ($z \sim 10 - 15$), from where the signal, however, is much weaker.

Signals caused by resonant scattering increases with opacity of halos like thermal ones, but decrease when radiation and gas temperatures increase. Hence, the warm halos ($T_K \sim 400$ K) are brighter in the HD rotational lines ($\nu_{obs} \sim 85$ GHz) caused by resonant scattering, while the hot halos ($T_K \sim 2000$ K) are brighter in the line of ortho-H₂ ($\nu_{obs} \sim 338$ GHz) caused by thermal collisions with hydrogen atoms.

The estimations of the differential brightness temperature caused by the resonant scattering in the first rotational levels of hydrogen deuteride molecule in the dark ages halos presented here are comparable with the values obtained by Núñez-López et al. (2006). They computed the secondary anisotropy of CMB caused by resonant scattering in HD lines of top-hat halos of the wide mass range $10^2 - 10^{12} M_\odot$ at the stages of their turn-around and after virialization. They have constrained themselves by analysis of the halos which are formed from the overdensity with the initial amplitude of relative density perturbations $\delta\rho/\bar{\rho} \sim 3\sigma$ and 6σ , where σ is the value of rms density perturbations at the corresponding scale.

We study the halos with initial amplitudes of curvature perturbations $C_k = 1.5 - 3 \cdot 10^{-4}$ (seed of halos) that are in the same range of peak heights (see section 2.1 in (Novosyadlyj et al. 2018)). The opacities in the rotational lines $J = 1 - 0, 2-1$ and $3-2$ in the left panel of Figure 5 and 9 for halos with mass of $5.3 \cdot 10^9 M_\odot$ and corresponding initial amplitudes are comparable with opacities computed by Núñez-López et al. (2006) (Figure 2 and 3) for the halos at their turn-around points (in our figures they are at $z = 46, 38, 30, 22$ and 15 for lines from top to bottom). The secondary anisotropy of CMB $\Delta T/\bar{T}$ caused by resonant scattering in halos at turn-around point computed by Núñez-López et al. (2006) is in the range $\sim 10^{-10} - 10^{-12}$ for the first rotational transition of HD molecule. Our computations give the values $\sim 3 \cdot 10^{-12} - 2 \cdot 10^{-14}$ for halos of mass $5.3 \cdot 10^9 M_\odot$ and initial amplitudes from the range $3-6\sigma$. They will be larger for the halos of larger masses. For the virialized halos Núñez-López et al. (2006) obtained $\sim 2 \cdot 10^{-5} - 10^{-8}$. Our estimations for hot halos fall within this range of values (Figure 6).

Since the peculiar velocities of different halos have a random amplitude and direction, the superposition of these effects gives the rms total amplitude of the differential brightness temperature $\langle \delta T_{ul}^b \rangle = \left[\langle (\delta T_{ul}^{b(th)})^2 \rangle + \langle (\delta T_{ul}^{b(rs)})^2 \rangle \right]^{1/2}$, where angle parenthesis means ensemble averaging.

7. CONCLUSIONS

We have analyzed the emission of dark ages halos in the lines of transitions between lowest rotational levels of hydrogen molecules, para-H₂, ortho-H₂ and HD. It was assumed that halos are homogeneous top-hat spheres formed from the cosmological density perturbations in the four-component Universe with post-Planck cosmological parameters. We have considered the excitation/de-excitation of lowest five rotational levels of hydrogen molecules by cosmic microwave background radiation and thermal collisions with atomic hydrogen. The kinetic equations for populations of the energy levels have been solved by two independent ways, which give the close final values of differential brightness temperatures of virialized halos caused by thermal collisions. The first one consists in the integration of system of differential kinetic equations for populations of the levels together with system of differential equations of evolution of cosmological perturbations and kinetic equations of formation/destruction of the first molecules. The results of numeric integration, presented in Figures 4-6 and 8-9 in Appendix of the on-line version, show the dependence of opacities and differential brightness temperatures on the redshift from the early stage of halo formation to virialized final stage. The second way of analysis consist in solution of system of algebraic equations for populations of the lowest rotational levels of molecules H₂ and HD in the virialized halos. These solutions give us a possibility to compute the excitation temperatures of levels, the differential brightness temperatures and fluxes in the lines of transitions between them, which are presented in Tables 3-8 and 15-16 in Appendix of the on-line version. Both ways give practically the same values for populations of levels, opacities, differential brightness temperatures and

spectral fluxes for virialized halos. We also compute the differential brightness temperatures and spectral fluxes in the same lines caused by resonant scattering of cosmic microwave background radiation for the halos with a root mean square value of peculiar velocity at different redshift. The results are presented in Tables 9-10 and in the last two columns of Tables 15-16 in Appendix of the on-line version.

The main conclusions issued from the obtained results are as follows. 1) The dark ages halos are source of emission in the lines of transitions between lowest rotational levels of hydrogen molecules excited by CMB radiation and collisions with atoms of neutral hydrogen. 2) The amplitudes of differential brightness temperatures caused by thermal collisions with H are systematically larger in the rotational lines of ortho-H₂ and para-H₂ molecules than in the lines of HD ones. The maximal values are reached for the earliest warm small halos ($z_v \sim 50$, $T_K \sim 800$ K, $M_h \sim 10^6 M_\odot$) but they do not exceed nano Kelvin at $\nu_{obs} \sim 200 - 300$ GHz. 3) The amplitudes of differential brightness temperatures in the lowest rotational lines of HD molecules caused by resonant scattering are systematically higher than caused

by thermal collisions with H for halos with peculiar velocity equal to rms one followed from the power spectrum of cosmological perturbations and directed to/from the terrestrial observer. The maximal values which are reached are about few nanokelvins at $\nu_{obs} \sim 85 - 170$ GHz for the massive warm halos ($z_v \sim 20$, $T_K \sim 200$ K, $M_h \sim 5 \cdot 10^9 M_\odot$). 4) If the dark ages halos are hot after virialization ($T_K \sim 2000 - 5000$) then the differential brightness temperatures caused by thermal collisions are increased by a few orders large, reaching the values in few microkelvins, that may be achievable for the next-generation telescopes.

This work was supported by the International Center of Future Science and College of Physics of Jilin University (P.R.China) and the project of Ministry of Education and Science of Ukraine "Formation and characteristics of elements of the structure of the multicomponent Universe, gamma radiation of supernova remnants and observations of variable stars" (state registration number 0119U001544). We acknowledge the anonymous referee for his accurate report and useful comments and suggestions.

REFERENCES

- Barkana, R., Loeb, A. 2001, Phys. Rep., 349, 125
 Basu, K. 2007, New Astron. Rev., 51, 431
 de Bernardis, P., Dubrovich, V., Encrenaz, P. et al. 1993, A&A, 269, 1
 Bowman, J.D., Rogers, A.E.E., Monsalve, R.A. et al. 2018, Nature, 555, 67
 Bromm, V. & Yoshida, N. 2011, Ann. Rev. A&A, 49, 373
 Carroll, S.M., Press, W.H. & Turner, E.L. 1992, Ann. Rev. A&A, 30, 499
 Chen, R. & McKeever, S.W. 1997, Theory of Thermoluminescence and Related Phenomena. World Scientific, Singapore, 400 p.
 Dubrovich, V. K. 1977, Sov. Astron. Lett., 3, 128
 Dubrovich, V., Bajkova, A., Khaikin, V. B. 2008, New Astron., 13, 28
 Eisenstein, D.J. & Hu, W. 1998, ApJ, 496, 605
 Fan, X., Carilli, C.L. & Keating, B. 2006, Ann. Rev. A&A, 44, 415
 Field, G. B., Somerville, W. B. & Dressler, K. 1966, Ann. Rev. A&A, 4, 207
 Flower, D.R. 1997, MNRAS, 288, 627
 Flower, D.R. & Roueff, E. 1998, J.Phys. B, 31, 955
 Flower, D. R. & Roueff, E. 1999, MNRAS, 309, 833
 Flower, D. R. & Pineau des Forêts, G. 2000, MNRAS, 316, 901
 Furlanetto, S.R., Oh, S. P. & Briggs, F.H. 2006, Physics Reports, 433, 181
 Goschinskij, I. V., Dubrovich, V. K., Zhelenkov, S. R., Ilin, G. N., & Prozorov, V. A. 2002, Astron. Rep., 46, 543
 Goss, W.M. & Field, G.B. 1968, ApJ, 151, 177
 Iliev, I.T., Shapiro, P.R., Ferrara, A. & Martel, H. 2002, ApJ, 572, L123
 Kamaya, H. & Silk, J. 2002, MNRAS, 332, 251
 Kamaya, H. & Silk, J. 2003, MNRAS, 339, 1256
 Lang, K. R. 1974, Astrophysical Formulae. A. Compendium for the Physicist and Astrophysicist. Springer-Verlag, Berlin, Heidelberg, New York, 760 p.
 Lique, F., Honvault, P. & Faure, A. 2012, J. Chem. Phys., 137, 154304
 Lique, F. 2015, MNRAS, 453, 810
 Maoli, R., Melchiorri, F., & Tosti, D. 1994, ApJ, 425, 372
 Maoli, R., Ferrucci, V., Melchiorri, F., & Tosti, D. 1996, ApJ, 457, 1
 Mizusawa, H., Omukai, K. & Nishi, R. 2005, Publ. Astron. Soc. Japan, 57, 951
 Novosyadlyj, B., Shulga, V., Han, W., Kulinich, Yu., & Tsizh, M. 2018, ApJ, 865, 38
 Novosyadlyj, B., Tsizh, M., Kulinich, Yu. 2016, Gen. Relativ. Grav., 48, 30
 Núñez-López, R., Lipovka, A. & Avila-Reese, V. 2006, 369, 2005
 Omukai, K. & Kitayama, T. 2003, ApJ, 599, 738
 Persson, C. M., R. Maoli, R., Encrenaz, P. et al. 2010, A&A, 515, A72
 Planck Collaboration: Akrami, Y., Arroja, F., Ashdown, M. et al. 2018, arXiv:1807.06205
 Planck Collaboration: Aghanim, N., Akrami, Y., Ashdown, M. et al. 2018, arXiv:1807.06209
 Pritchard, J.R. & Loeb, A. 2012, Reports on Progress in Physics, 75, id. 086901
 Purcell, E.M. 1952, ApJ, 116, 457
 Rogers, A.E.E. & Barrett, A.H. 1968, ApJ, 151, 163
 Roueff, E. & Flower, D. R. 1999, MNRAS, 305, 353
 Takayanagi, K. & Nishimura, S. 1960, PASJ, 12, 163
 Takayanagi, K. 1963, Progr. Theor. Phys. Suppl., 25, 1
 Wrathmall, S.A., Gusdorf, A. & Flower, D.R. 2007, MNRAS, 382, 133

APPENDIX A. TABLES AND FIGURES FOR THE ONLINE VERSION ONLY.

TABLE 11

PHYSICAL VALUES AND CHEMICAL COMPOSITION OF HALOS VIRIALIZED AT DIFFERENT z_v : M IS THE TOTAL MASS, C_k IS THE AMPLITUDE OF INITIAL CURVATURE PERTURBATION (SEED OF HALO), z_v IS THE REDSHIFT OF VIRIALIZATION, ρ_m IS THE MATTER DENSITY VIRIALIZED HALO, T_K IS KINETIC TEMPERATURE OF BARYONIC GAS, n_{HI} IS THE NUMBER DENSITY OF NEUTRAL HYDROGEN ATOMS, n_p, n_e ARE THE NUMBER DENSITIES OF PROTONS AND ELECTRONS AT $z = z_v/10$, n_{H_2} AND n_{HD} ARE THE NUMBER DENSITIES OF MOLECULES H_2 AND HD , r_h IS THE RADIUS OF HALO IN COMOVING COORDINATES, θ_h IS THE ANGULAR RADIUS OF GEOMETRICALLY LIMITED HALO.

M_h [M_\odot]	k [Mpc^{-1}]	C_k	z_v	ρ_m [g/cm^3]	T_K [K]	n_{HI} [cm^{-3}]	$n_p \approx n_e$ [10^{-6}cm^{-3}]	n_{H_2} [10^{-6}cm^{-3}]	n_{HD} [10^{-9}cm^{-3}]	r_h [kpc]	θ_h [']
$6.6 \cdot 10^8$	10	$3.0 \cdot 10^{-4}$	35.54	$2.40 \cdot 10^{-23}$	508.9	1.80	156.3/3.7	30.32	3.83	0.77	0.50
		$2.5 \cdot 10^{-4}$	29.41	$1.38 \cdot 10^{-23}$	382.8	1.04	97.4/3.8	12.41	2.36	0.92	0.52
		$2.0 \cdot 10^{-4}$	23.28	$7.05 \cdot 10^{-24}$	266.3	0.53	54.2/3.9	4.29	1.94	1.15	0.53
		$1.5 \cdot 10^{-4}$	17.17	$2.95 \cdot 10^{-24}$	162.1	0.22	25.1/4.2	1.18	0.98	1.54	0.56
		$1.0 \cdot 10^{-4}$	11.05	$8.60 \cdot 10^{-25}$	78.2	0.06	8.3/4.7	0.23	0.16	2.32	0.61
$8.3 \cdot 10^7$	20	$3.0 \cdot 10^{-4}$	40.57	$3.54 \cdot 10^{-23}$	619.2	2.65	214.5/3.7	58.54	6.24	0.34	0.25
		$2.5 \cdot 10^{-4}$	33.55	$2.03 \cdot 10^{-23}$	468.4	1.52	133.5/3.7	23.71	3.25	0.40	0.25
		$2.0 \cdot 10^{-4}$	26.54	$1.03 \cdot 10^{-23}$	325.5	0.77	74.0/3.8	7.96	2.10	0.51	0.26
		$1.5 \cdot 10^{-4}$	19.50	$4.24 \cdot 10^{-24}$	199.6	0.32	33.8/4.0	2.08	1.46	0.68	0.27
		$1.0 \cdot 10^{-4}$	12.36	$1.17 \cdot 10^{-24}$	94.0	0.09	10.4/4.5	0.36	0.30	1.05	0.30
$1 \cdot 10^7$	40	$3.0 \cdot 10^{-4}$	45.72	$5.01 \cdot 10^{-23}$	730.3	3.76	287.2/3.6	103.8	9.94	0.15	0.12
		$2.5 \cdot 10^{-4}$	37.85	$2.88 \cdot 10^{-23}$	556.0	2.16	179.7/3.7	40.91	4.78	0.18	0.13
		$2.0 \cdot 10^{-4}$	29.92	$1.46 \cdot 10^{-23}$	392.9	1.09	99.7/3.8	13.97	2.45	0.23	0.13
		$1.5 \cdot 10^{-4}$	22.02	$6.00 \cdot 10^{-24}$	242.8	0.45	45.7/3.9	3.53	1.80	0.30	0.13
		$1.0 \cdot 10^{-4}$	14.00	$1.66 \cdot 10^{-24}$	115.2	0.13	14.1/4.3	0.58	0.50	0.47	0.14
$1.3 \cdot 10^6$	80	$3.0 \cdot 10^{-4}$	50.33	$6.66 \cdot 10^{-23}$	834.0	5.00	355.3/3.6	172.5	15.40	0.068	0.061
		$2.5 \cdot 10^{-4}$	41.52	$3.78 \cdot 10^{-23}$	636.5	2.84	218.8/3.7	69.78	7.28	0.082	0.062
		$2.0 \cdot 10^{-4}$	32.65	$1.87 \cdot 10^{-23}$	446.8	1.41	117.7/3.7	23.12	3.25	0.10	0.064
		$1.5 \cdot 10^{-4}$	24.40	$8.07 \cdot 10^{-24}$	286.1	0.61	58.6/3.9	5.68	1.94	0.14	0.066
		$1.0 \cdot 10^{-4}$	15.38	$2.16 \cdot 10^{-24}$	134.4	0.16	17.1/4.2	0.89	0.78	0.21	0.071

TABLE 12

THE BEST-FIT COEFFICIENTS OF ANALYTICAL APPROXIMATION OF THE DEPENDENCES OF THE COLLISIONAL DEACTIVATION RATE COEFFICIENTS ON THE KINETIC TEMPERATURE T_K BY FORMULA $\lg \kappa_{ul}(T_K) = \sum_{k=0}^{N-1} a_k^{(ul)} (\lg T_K / \epsilon^{(ul)})^k + a_N^{(ul)} (1 / (T_K / \epsilon^{(ul)} + \epsilon^{(ul)}) - 1)$ FOR H_2 MOLECULE (SOLID LINES IN THE LEFT PANEL OF FIGURE 1). IT IS VALID IN THE TEMPERATURE RANGE $100 \leq T_K \leq 6000$ K. THE COEFFICIENTS ARE TAKEN FROM THE VAMDC BASEDATA, THE MISPRINTS IN THE FORMULA HAVE BEEN FIXED.

u	l	ϵ	a_0	a_1	a_2	a_3	a_4	a_5	a_6	a_7	a_8
2	0	6.0	-8259.36044	1846.12284	-4713.51503	3907.15150	-1672.56520	4015.80145	-51.6262545	2.78079268	-9095.89801
3	1	15.0	1402.43596	-58.1010752	74.2671058	18.8773370	-36.2141786	12.2012441	-1.32412404	0.00000000	1484.70110
4	2	15.0	11533.9595	2070.41178	-4153.50389	5002.05894	-3171.93991	1091.80410	-195.457394	14.3495151	12713.2249
5	3	13.0	5064.45306	73.5896891	-266.094034	722.660337	-590.299001	223.156022	-41.0457115	2.98641025	5439.61121
4	0	24.0	6887.91049	-219.803978	673.503903	-912.827587	802.461038	-395.623746	98.4201969	-9.67987032	7148.50271
5	1	61.0	76184.3307	76.4032424	-87.2258173	387.822432	-476.720251	397.196415	-157.426338	22.3504536	77451.1227

TABLE 13

THE BEST-FIT COEFFICIENTS OF ANALYTICAL APPROXIMATION OF THE DEPENDENCES OF THE COLLISIONAL DEACTIVATION RATE COEFFICIENTS ON THE KINETIC TEMPERATURE T_K BY QUADRATIC PARABOLA FOR H_2 MOLECULE FOR TEMPERATURE RANGE 50 -500 K (SOLID LINES IN THE LEFT PANEL OF FIGURE 1).

u	l	a_0	a_1	a_2
2	0	-14.653	0.066487	0.24931
3	1	-6.0491	-6.8089	1.6397
4	2	-9.5234	-3.7050	0.94767
5	3	-13.942	-1.0658	0.56254
4	0	-14.910	0.072763	0.14760
5	1	-18.092	0.14405	0.063031

TABLE 14

THE BEST-FIT COEFFICIENTS OF ANALYTICAL APPROXIMATION OF THE DEPENDENCES OF THE COLLISIONAL DEACTIVATION RATE COEFFICIENTS FOR HD MOLECULE ON THE KINETIC TEMPERATURE T_K BY POLYNOM OF 3D ORDER,
 $\lg \kappa_{ul}(T_K) = a_{ul} + b_{ul} \lg T_K + c_{ul} (\lg T_K)^2 + d_{ul} (\lg T_K)^3$ (SOLID LINES IN THE RIGHT PANEL OF FIGURE 1).

u	l	a	b	c	d
1	0	-16.026	-2.2319	1.2578	-0.17135
2	0	-12.813	-8.2155	3.6827	-0.46921
3	0	-6.1385	-16.448	6.3996	-0.74128
4	0	8.5527	-32.399	11.634	-1.2838
5	0	2.6510	-27.177	9.7365	-1.0395
2	1	-15.293	-2.7751	1.3979	-0.18162
3	1	-12.970	-7.7509	3.4431	-0.43110
4	1	-5.8105	-16.797	6.5236	-0.75144
5	1	-2.9747	-21.584	8.2829	-0.93604
3	2	-13.998	-4.3688	2.0205	-0.25961
4	2	-13.766	-6.9609	3.1745	-0.39987
5	2	-9.2775	-13.887	5.7245	-0.67937
4	3	-16.229	-2.2922	1.3529	-0.18594
5	3	-14.639	-6.3194	3.0045	-0.38352
5	4	-16.554	-2.3252	1.4452	-0.20237

TABLE 15

THE OPTICAL DEPTHS, BRIGHTNESS TEMPERATURES AND SPECTRAL FLUXES IN THE TWO LOWEST ROTATIONAL LINES OF MOLECULE H_2 IN THE DARK AGES HALOS OF DIFFERENT MASSES M_h VIRIALIZED AT DIFFERENT REDSHIFT z_v . MARKING (TH) MEANS THE THERMAL EMISSION, MARKING (RS) MEANS THE RESONANT SCATTERING.

M_h [M_\odot]	z_v	ν_{obs} [GHz]	$\Delta\nu_{obs}$ [kHz]	τ_ν 10^{-9}	$\delta T_{br}^{(th)}$ [10^{-12} K]	$\delta F^{(th)}$ [10^{-12} Jy]	$\delta T_{br}^{(rs)}$ [10^{-12} K]	$\delta F^{(rs)}$ [10^{-12} Jy]
1.29 $\cdot 10^6$	50.33	207	3.02	1.88	799.0	0.288	16.9	0.006
		343	4.99	13.1	657.0	0.650	28.1	0.028
	41.52	250	3.18	1.39	175.0	0.095	7.55	0.004
		414	5.27	7.44	91.1	0.136	6.05	0.009
	32.65	316	3.37	0.77	22.0	0.020	1.82	0.002
		523	5.58	3.76	7.49	0.019	0.63	0.002
	24.40	418	3.57	0.31	1.51	0.003	0.18	0.0003
		693	5.91	1.55	0.30	0.001	0.02	0.00009
	15.39	648	3.79	0.11	0.01	0.00005	0.002	0.00001
		1070	6.28	0.54	0.0008	0.00001	0.00002	0.0000002
1.04 $\cdot 10^7$	45.72	227	3.10	3.16	732.0	1.300	22.4	0.040
		377	5.14	18.7	468.0	2.280	25.4	0.124
	37.85	273	3.25	2.03	141.0	0.380	8.29	0.022
		453	5.39	10.3	61.9	0.458	4.82	0.036
	29.92	343	3.44	1.08	18.6	0.083	1.78	0.008
		569	5.69	5.29	5.45	0.066	0.45	0.005
	22.02	461	3.63	0.46	1.09	0.009	0.15	0.001
		764	6.01	2.31	0.18	0.004	0.01	0.00023
	14.00	708	3.83	0.18	0.006	0.0001	0.001	0.00003
		1170	6.35	0.82	0.0004	0.00002	0.000005	0.0000003
8.28 $\cdot 10^7$	40.57	255	3.21	4.91	545.0	4.990	24.9	0.229
		423	5.31	25.9	273.0	6.870	18.4	0.464
	33.55	307	3.36	2.98	103.0	1.420	7.88	0.109
		509	5.56	14.6	36.8	1.400	3.02	0.115
	26.54	386	3.51	1.52	12.5	0.288	1.41	0.033
		639	5.82	7.48	2.91	0.184	0.22	0.014
	19.50	518	3.69	0.67	0.61	0.028	0.093	0.004
		858	6.12	3.38	0.078	0.010	0.003	0.0004
	12.36	795	3.89	0.32	0.0029	0.0004	0.0006	0.00008
		1320	6.44	1.24	0.0001	0.00003	0.0000007	0.0000002
6.63 $\cdot 10^8$	35.54	291	3.31	6.82	330.0	16.1	22.4	1.09
		481	5.48	33.9	131.0	17.5	10.5	1.40
	29.41	349	3.45	3.96	61.5	4.53	6.04	0.445
		579	5.71	19.4	17.5	3.530	1.42	0.288
	23.28	437	3.60	2.03	7.27	0.893	0.91	0.112
		725	5.97	10.2	1.32	0.445	0.080	0.027
	17.17	585	3.76	0.96	0.27	0.065	0.050	0.012
		968	6.22	4.78	0.027	0.018	0.0008	0.00052
	11.05	881	3.93	0.52	0.0011	0.0007	0.0003	0.00017
		1460	6.52	1.84	0.00002	0.00004	0.0000001	0.0000002
5.30 $\cdot 10^9$	30.41	338	3.42	8.67	164.0	44.9	15.3	4.20
		560	5.67	42.4	49.2	37.0	4.11	3.09
	25.15	406	3.54	4.99	29.2	12.1	3.49	1.45
		673	5.87	24.8	6.13	6.98	0.43	0.494
	19.90	508	3.68	2.67	2.87	2.00	0.43	0.299
		842	6.10	13.5	0.38	0.729	0.017	0.032
	14.65	679	3.82	1.43	0.076	0.104	0.018	0.024
		1120	6.32	6.64	0.0051	0.019	0.00009	0.0003
	9.41	1020	3.98	0.94	0.00016	0.0006	0.00005	0.0002
		1690	6.60	2.60	0.00001	0.00001	0.000000003	0.00000003

TABLE 16

THE OPTICAL DEPTHS, BRIGHTNESS TEMPERATURES AND SPECTRAL FLUXES IN THE TWO LOWEST ROTATIONAL LINES OF MOLECULE HD IN THE DARK AGES HALOS OF DIFFERENT MASSES M_h VIRIALIZED AT DIFFERENT REDSHIFT z_ν . MARKING (TH) MEANS THE THERMAL EMISSION, MARKING (RS) MEANS THE RESONANT SCATTERING.

M_h	z_ν	ν_{obs}	$\Delta\nu_{obs}$	τ_ν	$\delta T_{br}^{(th)}$	$\delta F^{(th)}$	$\delta T_{br}^{(rs)}$	$\delta F^{(rs)}$
[M_\odot]		[GHz]	[kHz]	10^{-9}	[10^{-12} K]	[10^{-12} Jy]	[10^{-12} K]	[10^{-12} Jy]
1.29·10 ⁶	50.33	52.1	0.62	19.0	230.0	0.005	435.0	0.010
		104	1.23	21.4	65.4	0.006	401.0	0.036
	41.52	62.9	0.65	16.3	99.2	0.003	328.0	0.011
		125	1.30	14.4	21.5	0.003	217.0	0.030
	32.65	79.5	0.69	14.8	37.0	0.002	250.0	0.015
		158	1.38	9.13	5.30	0.001	98.2	0.023
	24.40	105	0.73	20.0	16.0	0.002	260.0	0.029
		210	1.46	7.25	1.20	0.0005	44.3	0.019
	15.39	163	0.78	25.9	2.69	0.0008	186.0	0.057
		325	1.55	3.09	0.044	0.00005	4.53	0.006
1.04·10 ⁷	45.72	57.3	0.64	33.1	285.0	0.032	713.0	0.08
		114	1.27	33.2	71.4	0.032	561.0	0.25
	37.85	68.9	0.67	28.4	121.0	0.021	537.0	0.92
		137	1.33	22.0	22.7	0.015	295.0	0.20
	29.92	86.5	0.71	28.7	51.6	0.015	451.0	0.13
		172	1.41	15.3	6.20	0.007	141.0	0.16
	22.02	116	0.74	49.0	25.6	0.014	570.0	0.31
		232	1.48	14.3	1.45	0.032	67.9	0.15
	14.00	178	0.79	41.6	2.75	0.041	253.0	0.38
		355	1.57	3.75	0.03	0.0002	3.68	0.022
8.28·10 ⁷	40.57	64.3	0.66	59.7	337.0	0.196	1190.0	0.69
		128	1.31	51.0	70.7	0.163	749.0	1.73
	33.55	77.4	0.69	54.8	153.0	0.134	944.0	0.83
		154	1.37	35.2	23.1	0.081	396.0	1.38
	26.54	97.1	0.72	69.1	77.0	0.113	973.0	1.42
		194	1.44	29.5	7.08	0.041	217.0	1.26
	19.50	130	0.76	109.0	33.9	0.097	1100.0	3.17
		260	1.51	24.1	1.33	0.015	81.3	0.93
	12.36	200	0.80	63.8	2.24	0.018	304.0	2.43
		399	1.59	3.86	0.013	0.0004	2.08	0.66
6.63·10 ⁸	35.54	73.2	0.68	109.0	376.0	1.160	1960.0	6.08
		146	1.35	76.7	63.1	0.777	940.0	11.6
	29.41	88.0	0.71	116.0	195.0	0.913	1800.0	8.41
		175	1.41	60.0	22.7	0.421	539.0	10.0
	23.28	110	0.74	182.0	120.0	0.939	2250.0	17.5
		220	1.47	59.8	7.98	0.247	327.0	10.1
	17.17	147	0.77	201.0	35.4	0.541	1700.0	26.0
		293	1.54	32.3	0.90	0.054	71.6	4.35
	11.05	222	0.81	88.5	1.68	0.069	328.0	13.5
		442	1.61	3.62	0.0053	0.0009	1.06	0.17
5.30·10 ⁹	30.41	85.2	0.70	225.0	428.0	7.44	3570.0	62.1
		170	1.40	123.0	53.2	3.68	1170.0	80.9
	25.15	102	0.73	317.0	284.0	7.48	4240.0	112.0
		204	1.45	122.0	22.9	2.40	798.0	83.5
	19.90	128	0.76	428.0	145.0	6.41	4420.0	195.0
		255	1.51	99.3	60.8	1.07	356.0	62.3
	14.65	171	0.78	312.0	25.9	2.25	2060.0	179.0
		341	1.56	32.3	0.34	0.12	38.6	13.4
	9.41	257	0.82	125.0	0.90	0.21	305.0	72.3
		512	1.63	2.74	0.001	0.0009	0.29	0.27